AD-A199 774 DYNAMICAL PROPERTIES OF SOLAR CURRENT LOOPS WITH LINE-TIED FOOTPRINTS: EFFECTS OF TOROIDAL FORCES(U) NAVAL RESEARCH LAB WASHINGTON DC J CHEN 25 AUG 88 NRL-MR-6256 1/1

UNCLASSIFIED F/G 3/2 NL

[redacted]

END
DATE FILMED
12 88

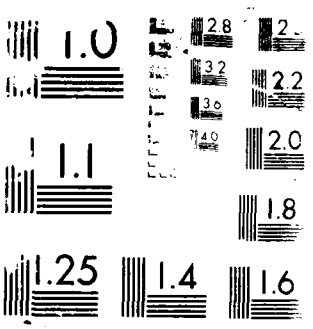
1.0
1.1
1.25
1.4
1.6
1.8
2.0
2.2
2.8
3.2
3.6
4.0

Naval Research Laboratory

Washington, DC 20375-5000

NRL Memorandum Report 6256

Dynamical Properties of Solar Current Loops with Line-Tied Footprints: Effects of Toroidal Forces

JAMES CHEN

Geophysical and Plasma Dynamics Branch
Plasma Physical Division

August 25, 1988

SECURITY CLASSIFICATION OF THIS PAGE

REPORT DOCUMENTATION PAGE

Form Approved OMB No. 0704-0188

1a REPORT SECURITY CLASSIFICATION UNCLASSIFIED	1b RESTRICTIVE MARKINGS
2a SECURITY CLASSIFICATION AUTHORITY	3 DISTRIBUTION/AVAILABILITY OF REPORT Approved for public release; distribution unlimited.
2b DECLASSIFICATION/DOWNGRADING SCHEDULE	
4 PERFORMING ORGANIZATION REPORT NUMBER(S) NRL Memorandum Report 6256	5 MONITORING ORGANIZATION REPORT NUMBER(S)
6a NAME OF PERFORMING ORGANIZATION Naval Research Laboratory	6b OFFICE SYMBOL (If applicable) Code 4720
6c ADDRESS (City, State, and ZIP Code) Washington, DC 20375-5000	7a NAME OF MONITORING ORGANIZATION 7b ADDRESS (City, State, and ZIP Code)
8a NAME OF FUNDING/SPONSORING ORGANIZATION Office of Naval Research	8b OFFICE SYMBOL (If applicable)
8c ADDRESS (City, State, and ZIP Code) Arlington, VA 22217	10 SOURCE OF FUNDING NUMBERS PROGRAM ELEMENT NO. / PROJECT NO. / TASK NO. / WORK UNIT ACCESSION NO.

11 TITLE (Include Security Classification)
Dynamical Properties of Solar Current Loops with Line-Tied Footprints: Effects of Toroidal Forces

12 PERSONAL AUTHOR(S)
Chen, James

13a TYPE OF REPORT	13b TIME COVERED	14 DATE OF REPORT (Year, Month, Day)	15 PAGE COUNT
Interim	FROM TO	June 30, 1987	

16 SUPPLEMENTARY NOTATION

17 COSATI CODES			18 SUBJECT TERMS (Continue on reverse if necessary and identify by block number)
FIELD	GROUP	SUB-GROUP	Coronal loop Current loop Solar physics

19 ABSTRACT (Continue on reverse if necessary and identify by block number)

An earlier paper reported a theoretical study of the effects of toroidal forces in current loops embedded in an ambient plasma such as the corona. These forces occur in current-carrying plasmas with curvature. The model loop is characterized by twisted magnetic field lines. The magnetic field and current density have toroidal and poloidal components. In this earlier work, a current loop was assumed to evolve while maintaining a half-torus configuration. The important geometrical constraint that footpoints are generally immobile on the relevant time scales was not taken into account. In the present paper, the dynamical properties of current loops similar to those of the earlier work are examined with the requirement that the footpoints remain stationary in the photosphere. Other essential ingredients of the model are unchanged. ~~It is found that~~ The behavior of the present, more realistic model is qualitatively similar to that of the earlier model. This is due to the fact that the toroidal forces have only a mild, logarithmic dependence on the local aspect ratio. In particular, the velocities which the apex can achieve under the action of toroidal forces and the magnetic energy

20 DISTRIBUTION/AVAILABILITY OF ABSTRACT	21 ABSTRACT SECURITY CLASSIFICATION
☒ SAME AS RPT. ☐ DTIC USERS ☐	UNCLASSIFIED
22a NAME OF RESPONSIBLE INDIVIDUAL James Chen	22b TELEPHONE (Include Area Code) (202) 767-3646

DD Form 1473, JUN 86

19. ABSTRACTS (Continued)

released in the form of drag heating are similar in their respective magnitudes. In the present calculation, the ratio η of the height of the apex and the footpoint separation is a physical parameter. It is found that a low-lying loop (small η) can evolve to a "taller" (larger η) loop in a quasi-equilibrium fashion if the current is increased slowly while holding the footpoint separation fixed. Time evolution of the loops and the magnetic energy converted via drag heating are presented. Results are also presented for loops with relatively strong current. The results are discussed in the context of the solar environment. ~~In particular~~, it appears that the toroidal forces can lead to a wide range of plasma motion. The accompanying drag heating can take place with a correspondingly wide range of rates.

DD Form 1473, JUN 86

CONTENTS

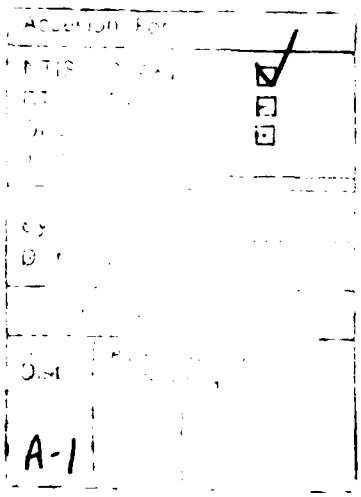

DYNAMICAL PROPERTIES OF SOLAR CURRENT LOOPS WITH LINE-TIED FOOTPRINTS: EFFECTS OF TOROIDAL FORCES

INTRODUCTION

In an earlier paper (Chen, 1987), the dynamical behavior of a current loop under the action of curvature ("toroidal") forces was studied. The model loop is immersed in an ambient plasma such as the corona and is characterized by twisted magnetic field lines. The magnetic field and current density have toroidal and poloidal components. The model assumes that the current conservation is established in or below the photosphere. The calculation showed that if the apex position of an equilibrium loop is perturbed, the loop can expand. The condition for instability to such expansion was given in terms of a parameter $\varepsilon \equiv \Phi_p/\Phi_T$, where Φ_p is the magnetic flux enclosed by the loop above the photosphere and Φ_T is the total flux of the entire current structure including the subphotospheric current. Although the subphotospheric flux or current structure is not measurable in reality, it is a physically meaningful quantity. The analysis used an integral form of $\underline{f} = c^{-1}\underline{J} \times \underline{B} - \nabla p$ to describe the center-of-mass motion of the apex. The drag between expanding loops and ambient gas was included using a simple model. This allows release of magnetic energy via drag heating. A less developed predecessor of this model was discussed by Xue and Chen (1980) in the context of a magnetic energy release mechanism.

The main results are the following. (1) There exists a critical value ε_{cr} which depends only on physical parameters above the photosphere such that an equilibrium loop with $\varepsilon < \varepsilon_{cr}$ ($\varepsilon > \varepsilon_{cr}$) is unstable (stable). (2) An unstable loop can expand and sometimes reach a "second" equilibrium following a period of damped small oscillation. A loop initially in equilibrium typically expands at subsonic velocities. This corresponds to slow drag heating of the ambient gas. (3) For a loop which is not initially in equilibrium (perhaps due to loss of equilibrium) with moderate to large current and magnetic fields, the apex can be driven supersonically through the ambient gas. For a loop with ~20G initially at a height of 10^5 km, the apex can attain velocities of roughly 1200 km s^{-1} for tens of minutes, dissipating up to 10^{32} erg via drag heating (also shock heating in the supersonic case). During the expansion of loops, the Lorentz force can do work so that the magnetic energy can be dissipated. Thus, a wide range of apex velocities and magnetic energy release rates are possible within the context of the model.

Manuscript approved June 3, 1988.

Curvature forces are a particular form of Lorentz and pressure forces which occur in curved segments of current-carrying plasmas and act along the local radius of curvature. (A similar force also occurs in metallic current hoops.) In the laboratory, these forces are well-understood. However, laboratory plasmas are typically surrounded by vacuum which in turn is enclosed in rigid metallic containers. In addition, magnetic fields are applied by external coils to balance the curvature forces (sometimes referred to as the "hoop stress"). In the solar and astrophysical environments, magnetic structures are usually embedded in plasmas and are not surrounded by metallic containers. The curvature forces in such environments have not been fully investigated.

The model described above was simplified in order to elucidate the basic physics underlying curvature forces and their effects in solar and astrophysical environments. One simplification is that the initial geometry of the loop is a half-torus of uniform aspect ratio R/a, where R is the major radius and a is the minor radius and that the loop expands (if unstable) maintaining the half-torus geometry. The uniform aspect ratio approximation is not expected to result in a serious error since the curvature forces depend on the local aspect ratio R/a as ln(8R/a), a relatively mild dependence. However, in a realistic current loop, the footpoints are expected to be essentially immobile compared with the apex on the relevant time scale of tens of minutes (the so-called photospheric "line tying") and the loop does not remain a half torus. In the ideal MHD approximation, the footpoint magnetic field is tied to the "infinitely" conducting photospheric (and subphotospheric) plasma which is much denser than the coronal plasma. In this paper, we achieve stationary footpoints without invoking the ideal MHD line tying because of the small fractional ionization in the photosphere (perhaps 10^{-3} to 10^{-4}). However, the ionized component of the photospheric plasma is coupled to the magnetic field lines that enter the photosphere. The ionized particles in turn are coupled to the neutrals via collisions on the relevant time scale. If the magnetic flux structure extends deeper down, the fractional ionization is expected to increase. Thus, any motion of the footpoints would be resisted by drag forces which scale as $n_p V_f^2$ (eq. [30]) where n_p is the photospheric density and V_f is the footpoint velocity. Since n_p is much greater than the coronal density n_c, the footpoint motion due to similar forces must be slower by $(n_c/n_p)^{1/2}$ in comparison with possible motions of the apex. If we estimate $n_c \sim 10^9$ cm^{-3} and $n_p \sim 10^{17}$ cm^{-3}, then $(n_c/n_p)^{1/2} \sim 10^{-4}$.

In the present paper, we will use a simple model geometry that explicitly takes into account the immobile footpoints. The basic physics is the same as that of the earlier paper (Chen, 1987). Because the more realistic geometry requires extensive modification of equations, it seems desirable to document the calculation in detail. We therefore repeat the analysis with immobile footpoints. However, the interested reader is referred to the earlier paper for a more general discussion of curvature forces in the solar environment and a more comprehensive reference list.

We will start with a model current loop which is initially in equilibrium and calculate its time-dependent behavior in response to perturbations of the apex height (Sec. II). The theoretical framework will be first presented, followed by a numerical calculation of the long-time evolution of loops including the drag force due to the ambient gas (Sec. III). Curvature forces are not limited to equilibrium loops. As an example, we discuss the behavior of a loop carrying a relatively large current, which may not be in equilibrium initially. Although no attempt to model specific observation will be made, we will discuss the potential relevance of the results to plasma activities in the corona (Sec. IV). It will be shown that a current loop acting under the influence of curvature forces can exhibit a range of behavior (expansion velocity, energy release, etc.) compatible with certain motion related effects in the solar environment.

II. DYNAMICS OF A MODEL CURRENT LOOP

In this section, we consider the evolution of an isolated loop with twisted magnetic field lines which is initially in equilibrium. Figure 1 shows schematically a model loop which has a toroidal magnetic field B_t and poloidal magnetic field B_p with a poloidal and toroidal current density components J_p and J_t, respectively. The apex of the loop is at a height of Z from the photosphere, R is the local radius of curvature (major radius) and a is the minor radius. The aspect ratio R/a is taken to be roughly 5 to 10. The loop is embedded in a field-free plasma of pressure p_a. In order to satisfy current conservation, we allow the current to close in or below the photosphere where the plasma is simply assumed to be much denser than the coronal plasmas. The footpoints are separated by a distance $2s_o$ and are assumed to be essentially immobile because of the dense subphotospheric plasmas. No particular current distribution will be specified below the photosphere.

The ambient plasma above the photosphere is assumed to decrease exponentially with a scale height H. In the corona, H can be given by

$$H = \frac{2kT_a}{m_i g} ,$$

where k is the Boltzman constant, T_a is the ambient plasma temperature, m_i is the ion mass and g is the gravitational acceleration which is 2.7×10^4 cm sec^{-2} at the surface. At the base of the corona, H is roughly 10^5 km.

A. Curvature forces

Curvature forces can occur in any curved segments of current-carrying plasmas and depend on the local major radius R and local minor radius a. In a solar loop configuration, we expect the apex region, say, one third of the loop about the apex, to exhibit the greatest degree of motion because it is farthest from the nearly immobile footpoints. The motion of the apex region, schematically shown in Figure 1 as the region between the two dashed lines, is determined by the Lorentz force, which consists of both the magnetic tension and pressure forces, and ∇p. The local force density $\underset{\sim}{f}$ acting on a plasma element is given by

$$\underset{\sim}{f} = \frac{1}{c} \underset{\sim}{J} \times \underset{\sim}{B} \quad \nabla p, \qquad (1a)$$

with the usual equation relating the current and magnetic field

$$\underline{J} = \frac{c}{4\pi} \underline{\nabla} \times \underline{B}. \tag{1b}$$

In this paper, the displacement current is neglected. Each plasma element moves according to $\underline{f}$. However, the motion of the center of mass of each segment of the loop is determined by the force integrated over the given segment. In considering the motion of the loop apex, we will refer to this center-of-mass motion. The center of mass of a slice of the loop lies on the dash-dot line along the loop. In order to integrate $\underline{f}$ over segments of the loop, we make a geometrical simplification that the loop above the photosphere is a part of a toroidal plasma which is intersected by the photosphere with a footpoint separation of $2s_o$. The current in or below the photosphere, which conserves current, will not be specified in detail. For such configurations, we see from Biot-Savart law that the contribution to the magnetic field near the apex due to the current segment below the photosphere scales as $(a/R)\theta/\pi$, where θ is the angle between the vertical and the line connecting a footpoint to the axis of the torus (see Fig. 1 and the definition of θ following eq. [11]). In view of this simplification, we will generally consider loops which are larger than half-torus for a given secant $2s_o$. Then, θ/π is less than 1/2. Because we consider R/a in the range of 5 to 10, $a/R \ll 1$. As the apex height increases, the loop becomes more toroidal with decreasing $\theta/\pi \ll 1$, reducing the correction term. The treatment is expected to be most accurate for curvature forces near the apex which remains nearly semi toroidal. This approximation is similar to that used by Anzer (1978) and Van Tend (1979). This geometry is an over-simplification but it has the advantage that we can analytically calculate the forces acting on segments of the loop near the apex and include the important feature that the footpoints are immobile. For an improved geometry, see, for example, Anzer and Poland (1979). Note that the integral form of $\underline{f}$ takes into account the curved geometry in a natural way.

In order to determine the motion of the apex (i.e., its center of mass), we integrate $\underline{f}$ over a section of the torus at the apex. In doing so, we must impose certain conditions: the loop is surrounded by a plasma of pressure p_a (no metallic container surrounding the loop) and the magnetic field vanishes at infinity. A technique for integrating over toroidal plasmas was developed previously (Shafranov, 1966), originally for

application to laboratory plasmas, and the analysis will not be reproduced here. Using the same analysis but with the above conditions (as opposed to the laboratory conditions), integration of $\underline{f}$ over a section of the torus yields the equation of motion for the center of mass of the apex

$$F_R = \frac{I_t^2}{c^2 R}\left[\ln\left(\frac{8R}{a}\right) + \frac{1}{2}\beta_p - \frac{1}{2}\frac{B_t^2}{B_p^2} - 1\right], \tag{2}$$

where $F_R = Md^2Z/dt^2$ with $M = \pi a^2 \bar{n} m_i$. Here F_R is the integrated force along the major radius per unit length of the loop. As the apex moves, the minor radius a also changes. This evolution can be described by

$$\frac{da^2}{dt^2} = \frac{I_t^2}{\pi c^2 a^3 \bar{n} m_i}\left(\frac{B_t^2}{B_p^2} - 1 + \beta_p\right). \tag{3}$$

Note that, for the simplified geometry, the major radius R is related to the height of the apex Z by

$$R = \frac{Z^2 + s_o^2}{2Z}. \tag{4}$$

This equation expresses the constraint that the footpoints are immobile. Here I_t is the total toroidal current defined by

$$I_t = 2\pi \int_0^a dr\, J_t.$$

The quantity β_p is defined by

$$\beta_p = \frac{\bar{p} - p_a}{B_p^2/8\pi}, \tag{5}$$

where $\bar{p}$ is the average internal pressure of the loop, p_a is the ambient pressure and $B_p = B_p(a)$ is the poloidal magnetic field at the outer edge of the loop ($r = a$). The quantity ξ_i is the internal inductance, characterizing the minor radial current distribution, and ξ_i ranges from 0 for a surface distribution to 1/2 for a uniform current distribution. Note that the curvature effects are relatively insensitive to the assumption of uniform R/a because of the logarithmic dependence. In equation (2), mass flow along the loop, orthogonal to major radial expansion, is also

neglected because the curvature forces occur with or without such flow. Moreover, mass flow is important only if the flow velocity is comparable to the Alfven speed in the loop.

By choosing to use the integrated form of the force equations, we sacrifice the description of each plasma element. However, this is not a serious disadvantage. In fact, if we were to obtain a local solution for each plasma element, we would integrate the result to determine quantities such as the center-of-mass motion in order to compare with observation. The integrated result would then take on the form of equations (2) and (3). The detailed structure enters through quantities such as $\bar{p}$ and ξ_i. This technique allows one to obtain the integrated form without first finding a detailed point-wise solution. The fact that MHD is amenable to global integrated representations has proved useful for various problems (e.g., energy principles, virial theorem, etc).

In Sec. III, we will integrate these equations numerically. In this section, we will first use a simplified version, applicable to near equilibrium cases, in order to study the linear behavior and gain insight for the later results. Note that if the loop is nearly in equilibrium, force balance along the minor radius, $da^2/dt^2 = 0$, gives

$$\beta_p \simeq 1 - B_t^2/B_p^2. \tag{6}$$

Substituting this expression into equation (2), we obtain

$$F_R \simeq \frac{I^2 t}{c^2 R}\left[\ln\left(\frac{8R}{a}\right) + \beta_p - \frac{3}{2} + \frac{\xi_i}{2}\right], \tag{7}$$

which describes the force per unit length of the loop acting on the center of mass if the loop is near equilibrium. As the initial configuration, we will adopt a model loop of the type discussed in Xue and Chen (1981). For this class of equilibrium loops, the curvature forces are explicitly balanced. Here, we give a brief summary of equilibrium properties. In equilibrium, the force density f acting on each element of the loop is zero. Therefore, we have $F_R = 0$ exactly. This equation then gives

$$\beta_p = \ln\left(\frac{8R}{a}\right) + \frac{3}{2} - \frac{\xi_i}{2}.$$

Since $\xi_i/2$ is generally the smallest term, we will adopt, for convenience, a surface current model and set $\xi_i = 0$ henceforth. For R/a of the order of 10, we see that $\beta_p < 0$ in equilibrium. This particular equilibrium condition arises from the absence of ambient magnetic field. This point and some modifications due to the presence of ambient fields will be discussed briefly in Sec. IV. However, the essential physics of curvature forces is not limited to this class of equilibria or by this condition. It is convenient to define the total poloidal current by

$$I_p = \int_0^a J_p dr ,$$

where the integration is over the minor radius. For the surface current model, we have

$$B_t = \frac{4\pi}{c} I_p$$

with $B_p = 0$ and $p = p_a$ inside the loop. Outside the loop, we have

$$B_p = \frac{2I_t}{cr}$$

with $B_t = 0$ and $p = p_a$ and r is measured along the minor radius from the center of the circular cross section. In the above expressions, the correction terms of the order $(a/R)\theta/\pi$ due to the geometrical simplification are neglected.

The above expressions are appropriate for current carrying plasmas embedded in an ambient plasma with no metallic containers. As noted before, this is an important difference from such laboratory systems as tokamaks. Incidentally, this class of equilibria properly satisfies the requirements of the virial theorem (Shafranov 1966).

B. Dynamical Instability

In this section, we investigate the stability properties of the equilibrium loop with respect to perturbations of the apex height. In Sec. III, we will consider more general cases with larger velocities. In the present paper, we will assume for simplicity that R/a is uniform. We note that the curvature forces depend on the local aspect ratio as $\ln(8R/a)$, which is a rather mild dependence, so that the essential physics of

curvature forces should not depend sensitively on this approximation. As the apex is displaced from its initial equilibrium, the forces experienced by the apex region be given by linearizing equation (7) which is valid for small deviation away from equilibrium;

$$\frac{d^2(\delta Z)}{dt^2} = \frac{I_t^2}{c^2 M \kappa}\left(\frac{Z}{R}\frac{dR}{dZ} - \frac{Z}{a}\frac{da}{dZ} + Z\frac{d\beta_p}{dZ}\right)\frac{\delta Z}{Z} . \qquad (8)$$

Here $M = \pi a^2 \rho$ is the mass per unit length of the loop, δa is the change in the minor radius and $\bar{\rho}$ is the average mass density inside the loop. The quantity $\delta\beta_p$ is obtained from eq. (5):

$$\delta\beta_p = \frac{\delta p - \delta p_a}{B_p^2/8\pi} - 2\beta_p \frac{\delta B_p}{B_p} , \qquad (9)$$

where δp is the change in the average internal pressure and

$$\delta p_a = \frac{\delta Z}{H} p_a , \qquad (10)$$

where H is the gravitational scale height. Because we assume that there is no mass flow along the loop, the total mass M_T of the loop above the photosphere is constant in time where

$$M_T = 2\pi\Theta R M ,$$

with M given above. Here, the function Θ is given by

$$\Theta \begin{cases} 1 & Z \geq s_o \\ \frac{\theta}{\pi} & Z < s_o \end{cases} \qquad (11)$$

where $\theta = \sin^{-1}(s_o/R)$ and $2\pi\theta R$ is the length of the loop above the photosphere. In this paper, we will mainly use $Z \geq s_o$. Because we use the integrated solution rather than the local (differential) solution, we will use a number of global conditions to constrain the dynamical behavior. We assume that, on the time scale of the loop evolution, possible changes in the fluxes are small. For the toroidal flux, we assume

$$B_t a^2 \tilde{=} \text{constant} \tag{12}$$

and for the poloidal flux, we assume

$$L_T I_t = \Phi_T \tilde{=} \text{constant}. \tag{13}$$

Here, Φ_T is the total poloidal flux and L_T is the total self-inductance of the current distribution including the submerged part (Figure 1). Note that current conservation requires only that there be some current. Given a current, the total flux Φ_T and inductance L_T can be unambiguously defined (albeit not necessarily measurable) without specifying details of the underlying current structure. The submerged structure is included in the calculation via the inductance. We can define the inductance L_p associated with the poloidal flux above the photosphere by

$$L_p \equiv \frac{\Phi_p}{I_t}$$

where the total poloidal flux is $\Phi_T = \Phi_p + \Phi_s$. Then, we define at time t

$$\varepsilon \equiv \frac{\Phi_p}{\Phi_T} = \frac{L_p}{L_T} . \tag{14}$$

This quantity ε is a rough measure of the relative "size" of the loop above the photosphere and the entire current structure. If the current is closed near the photosphere, then $\varepsilon \tilde{=} 1$. If the submerged current structure is much larger than the loop above, then $\varepsilon << 1$. Note that the initial flux Φ_s, thus the initial inductance of the submerged current, is not calculated. It is used as a parameter to characterize the submerged current structure. Note also that we do not require Φ_p and Φ_s to be separately constant since flux emergence appears to be common.

We have described the essential ingredients of the model. We will now attempt to calculate more specific properties. For the dynamics of the loop interior, we assume that the adiabatic expansion law is valid:

$$\bar{p}\ \bar{V}^{\gamma} \tilde{=} \text{constant}$$

where γ is the adiabatic index and where $\bar{V} = 2\pi^2 a^2 \Theta R$ is the volume of the

loop. Then, we have

$$\delta\bar{p} = -\gamma\bar{p}\left(2\frac{1}{a}\frac{da}{dZ} + \frac{1}{R}\frac{dR}{dZ} + \frac{1}{\Theta}\frac{d\Theta}{dZ}\right)\delta Z \ . \tag{15}$$

From equations (4) and (11), we obtain

$$\frac{Z}{R}\frac{dR}{dZ} = \frac{Z^2 - s_o^2}{Z^2 + s_o^2} \leq 1$$

and

$$\frac{d\Theta}{dZ} = \frac{1}{\pi}\frac{2s_o}{Z^2 + s_o^2} \ .$$

Next, from toroidal flux conservation, equation (12), we obtain

$$\frac{\delta B_t}{B_t} = -2\frac{\delta a}{a} \ . \tag{16}$$

From the definition of B_p, we find

$$\frac{\delta B_p}{B_p} = \frac{\delta I_t}{I_t} - \frac{\delta a}{a} \ . \tag{17}$$

In calculating δI_t, we assume that the submerged current structure, whatever it is, remains unchanged on the relevant time scale in the much denser plasma. This assumption is consistent with equation (4), the immobile footpoints. Then, the changes in L_T are primarily due to changes in the loop above the photosphere and we have

$$\delta L_T \cong \delta L_p .$$

From equation (13), we obtain

$$\frac{\delta I_t}{I_t} = -\varepsilon(t)\frac{\delta L_p}{L_p} \ . \tag{18}$$

For a partial-toroidal plasma of major radius R and minor radius a (R/a >> 1), the inductance is (Bateman, 1978)

$$L_p = \frac{4\pi\Theta R}{c^2}\left[\ln\left(\frac{8R}{a}\right) - 2\right] \tag{19}$$

with $\xi_i = 0$. Substituting the variation of L_p into equation (17), we find

$$\frac{\delta I_t}{I_t} = -\varepsilon\left[\frac{1}{R}\frac{dR}{dZ} + \hat{L}^{-1}\left(\frac{1}{R}\frac{dR}{dZ} - \frac{1}{a}\frac{da}{dZ}\right) + \frac{1}{\Theta}\frac{d\Theta}{dZ}\right]\delta Z ,$$

where $L = \ln(8R/a) - 2$. In order to determine da/dZ, we must related the changes in the pressure to changes in the field. From equations (6), (16) and (17), we obtain

$$\delta\beta_p = 2\left(1 - \beta_p\right)\left[-\varepsilon\left(1 + \hat{L}^{-1}\right)\frac{1}{R}\frac{dR}{dZ} - \varepsilon\frac{1}{\Theta}\frac{d\Theta}{dZ} + \left(1 + \varepsilon\hat{L}^{-1}\right)\frac{1}{a}\frac{da}{dZ}\right]\delta Z .$$

Equating this expression to the right hand side of equation (9) and using equations (10), (15) and (17), we can solve for da/dZ. After some straightforward algebra, we find

$$\frac{da}{dZ} = \frac{a}{2Z}\left[\varepsilon\hat{L}^{-1} + \left(1 - 2\beta_p\right) + \psi\right]^{-1}$$

$$\times\left[2\varepsilon\left(1 + \hat{L}^{-1}\right)\frac{Z}{R}\frac{dR}{dZ} + \frac{8\pi}{B_p^2}\left(\frac{Z}{H}p_a - \gamma\bar{p}\,\frac{Z}{R}\frac{dR}{dZ}\right) + \frac{Z}{\Theta}\frac{d\Theta}{dZ}\left(2\varepsilon - \psi\right)\right], \tag{20}$$

where

$$\psi \equiv \frac{\gamma\bar{p}}{B_p^2/8\pi} .$$

For the parameter values to be used later, this quantity ranges from 0.01 to 0.1. This means that the minor radius expansion is generally much slower than the apex motion. Using these results in equation (8), we finally obtain the linearized equation for the height of the apex:

$$\frac{d^2(\delta Z)}{dt^2} = \Gamma(t)\delta Z,$$

where

$$\Gamma(t) = \frac{I_t^2}{c^2 MR}\left\{\left[1 - 2\varepsilon\left(1 - \beta_p\right)\right]\frac{1}{R}\frac{dR}{dZ} + \left[2\left(1 - \beta_p\right)\left(1 + \varepsilon L^{-1}\right) - 1\right]\frac{1}{a}\frac{da}{dZ}\right.$$

$$\left. - 2\varepsilon\left(1 - \beta_p\right)\frac{1}{\Theta}\frac{d\Theta}{dZ}\right\} . \qquad (21)$$

Here $M = \pi a^2 \bar{n} m_i$ is the mass per unit length. If we set $\varepsilon \simeq 0$ ($\Phi_s >> \Phi_p$), the right hand side is positive, indicating that the perturbation grows. If we set $\varepsilon \simeq 1$ (the current is closed in the photosphere), the right hand side is negative so that the displacement is restored. Thus, there exists a quantity ε_{cr} with

$$0 < \varepsilon_{cr} < 1 \qquad (22)$$

such that the $d^2(\delta Z)/dt^2 = 0$ for $\varepsilon = \varepsilon_{cr}$. By setting $\Gamma(t=0)$ equal to zero and after some algebra, we find

$$\varepsilon_{cr} = -\left[q_1 \frac{Z}{R}\frac{dR}{dZ} - q_2\left(\psi\frac{Z}{\Theta}\frac{d\Theta}{dZ} - \eta\right)\right] \times \left\{\left[L^{-1} - q_3\left(1 + L^{-1}\right)\right.\right.$$

$$\left.\left. - q_4\psi\right]\frac{Z}{R}\frac{dR}{dZ} \quad \left(q_3 + q_4\psi\right)\frac{Z}{\Theta}\frac{d\Theta}{dZ} + q_4\eta\right\}^{-1} . \qquad (23)$$

Here we have defined $\eta \equiv (8\pi/B_\theta^2)(Z/H)p_a$, $q_1 \equiv (1 - 2\beta_p) + 1/2(1 + 2\beta_p)\psi$, $q_2 \equiv 1/2(1 - 2\beta_p)$, $q_3 \equiv (1 - 2\beta_p)^2 + 2(1 - \beta_p)\psi$, and $q_4 \equiv (1 - \beta_p)L^{-1}$. Note that ε_{cr} is a function of equilibrium quantities above the photosphere only. A current loop with $\varepsilon < \varepsilon_{cr}$ is unstable to perturbations and a loop with $\varepsilon > \varepsilon_{cr}$ is stable. For solar current loop parameters (e.g., $Z \sim 10^5$ km, $a \sim 10^4$ km, $p_a \sim$ a few dynes cm^{-2}), ε_{cr} is typically 0.2 to 0.4 (Sec. III). The quantities ε and ε_{cr} have the following physical interpretation. For $\varepsilon < \varepsilon_{cr} << 1$, the loop above the photosphere is a small fraction of the entire current distribution. As the loop expands, the changes in the loop magnetic field and average internal pressure are relatively small in comparison with the changes in the ambient pressure. In particular, $\delta\beta_p > 0$ so that the loop is unstable. For $\varepsilon > \varepsilon_{cr}$, the loop is a larger fraction of the total current. The magnetic field and internal pressure decrease more rapidly in such a way that the displacement is restored. In a more formal sense, the present time-dependent problem requires specification of

initial conditions. Given a loop above the photosphere, the quantity $\varepsilon(t=0)$ parametrizes the initial configuration according to the submerged current structure. This basic behavior depends on the existence but not the details of the submerged current structure which behaves differently from the loop above (i.e., much less mobile).

For the unstable case, equation (21) yields the exponential growth time τ is given by

$$\tau = \left[\Gamma(0)\right]^{-1/2}. \tag{24}$$

It is significant to note that $\tau \propto I_t^{-1}$ so that unstable loops with larger I_t linearly grows faster. For the stable case, the loop can oscillate about the equilibrium position.

At this point, it is useful to consider the energy budget of a current loop and provide a more transparent meaning for the terms in equation (7). Assuming, for simplicity, that the loop is a half-torus, the total magnetic energy of the semi-toroidal loop above the photosphere is the sum of the poloidal magnetic energy E_p and toroidal magnetic energy E_t where

$$E_p = \frac{1}{2} L_p I_t^2, \tag{25}$$

where L_p given by equation (19), and

$$E_t = \frac{B_t^2}{8\pi} \left(\pi^2 a^2 R\right). \tag{26}$$

Using the principle of virtual work, we find

$$F_p = \frac{\pi I_t^2}{c^2} \left[\ln \left(\frac{8R}{a}\right) - 1\right], \tag{27}$$

and

$$F_t = \frac{\pi I_t^2}{2c^2} \left(\beta_p - 1\right), \tag{28}$$

where F_p and F_t are the major radial forces acting on the entire loop due to $J_t B_p$ and $J_p B_t$, respectively. It is straightforward to show that the total pressure force in the major radial direction is

$$F_{\nabla p} = \frac{\pi I_t^2}{2c^2} \beta_p . \qquad (29)$$

Figure 2 shows the various local force components. Locally, the two components of the Lorentz force are both along the minor radius as shown. However, when these forces are integrated over the toroidal volume, we see that $J_t B_p$ contribution points outward along the major radius (eq. [27]) and $J_p B_t$ contribution points inward (eq. [28]). This is entirely due to the curvature of the current distribution. Adding the three forces and dividing the sum by πR to get the total force per unit length, we recover equation (7), providing a heuristic derivation. The expression for F_p shows that as the major radius expands, the B_p component does work on the loop, losing energy to the loop. At the same time, the loop does work on the B_t component so that the B_t component gains energy as the loop expands. Because the minor radius expands, the internal gas and B_t do work against the ambient pressure and lose energy. On balance, there is a net loss of poloidal magnetic energy to the kinetic energy of the loop. A fraction of this energy is then converted to thermal energy via drag heating.

C. The Behavior of an Expanding Current Loop

In the preceding section, we have described the near equilibrium behavior of a model current loop embedded in a background plasma. In this section, we will consider the long time scaling behavior which will be useful for interpreting the numerical results to be obtained.

As the loop expands, the velocity of the apex increases and the drag on the ambient gas becomes important. As a simple model, we write

$$F_d = c_d \left(n_a m_i a V^2 \right), \qquad (30)$$

where F_d is the drag force per unit length, $V = dZ/dt$ is the velocity of the loop (i.e., the apex), n_a is the local ambient density and c_d is the drag coefficient. An order-of-magnitude estimate for the characteristic terminal velocity in the nonlinear expansion phase can be obtained by equating F_d to the driving force F_R given by equation (7). We then obtain

$$V_* \sim I_t \left(c_d m_i c^2 n_a a R \right)^{-1/2} . \qquad (31)$$

Equation (31) shows that $V_\star$ is proportional to $I_t/n_a^{1/2}$. If we estimate $V_\star$ by taking $I_t \simeq 5 \times 10^{10}$ A, $n_a \simeq 4 \times 10^9$ cm^{-3}, $R \simeq 10^5$ km, $a \simeq 10^4$ km and using $c_d \simeq 1$, we find $V_\star \sim 2 \times 10^2$ km sec^{-1}. It is of interest to compare this value to the estimated sound speed C_s in the corona:

$$C_s \simeq \left(\gamma \frac{2kT_a}{m_i}\right)^{1/2}.$$

For $T_a \sim 2 \times 10^6$ K and $\gamma = 5/3$, $C_s \simeq 2.3 \times 10^2$ km sec^{-1}. Although the actual expansion velocity depends on ε, the above comparison indicates that the peak expansion velocity can be comparable to the sound speed under the action of curvature forces alone. It will turn out that equilibrium loops of the type used here can only produce subsonic expansion. However, if a loop is allowed to be out of equilibrium initially, carrying a sufficiently large I_t (e.g., loss of equilibrium at $t = 0$), then it may be driven supersonically (or super-Alfvenically for magnetized ambient plasmas).

III. EVOLUTION OF MODEL CURRENT LOOPS

In the preceding sections, we have discussed in detail the linear ($\delta Z/Z << 1$) behavior of a model current loop in a background plasma. The description of the long-time behavior has been limited to scaling laws. We will now attempt to provide a more quantitative discussion of the nonlinear behavior by numerically integrating the equations of motion. Numerical examples are given to illustrate the range of behavior under the action of curvature forces using parameters compatible with the solar environment. The basic physics, however, is not limited to the sun.

As the apex rises with increasing velocity, equation (7) will no longer be adequate. In addition, the drag due to the ambient plasma gas may become significant. We will incorporate this effect by a simple drag model, equation (30). Adding F_d to equation (2), we obtain

$$\frac{d^2Z}{dt^2} = \frac{I_t^2}{\pi c^2 a^2 R \bar{n} m_i}\left[\ln\left(\frac{8R}{a}\right) + \frac{1}{2}\beta_p - \frac{1}{2}\frac{B_t^2}{B_p^2} - 1\right] - c_d\left(\frac{2a n_a m_i}{\pi M}\right)V^2, \tag{32}$$

where $M = \pi a^2 \bar{\rho}$. Higher order contributions are neglected for simplicity. We have directly integrated the set of equations (3) and (32) for a variety of loop parameters. As stated in connection with equation (20), da/dt is typically one tenth of dZ/dt or less so that the minor radius is nearly in equilibrium for small to moderate dZ/dt. We have found equation (6) to be nearly true even for velocity V up to $0.5C_s$. This justifies, a posteriori, the use of equation (6) in the linear perturbation analysis.

The drag term in equation (32) is the force which the expanding loop experiences in displacing the ambient gas. The drag coefficient c_d is the coupling coefficient between the loop and the ambient medium. In our model, we adopt a simple c_d based on a straight cylinder transverse to the flow in a compressible gas. For the subsonic regime with a Reynolds number R_e of 10^6 to 10^8, c_d is 0.5 to 1 (Tritton 1977). At Mach 1, c_d attains a maximum value of approximately 2 and decreases rapidly for larger Mach numbers. The supersonic drag coefficient is obtained from Hoerner (1951).

In our calculation, the ambient plasma has no background field. If there are ambient magnetic fields, the drag coefficient c_d must be modified and, for super-Alfvenic motion, MHD shocks are generated. We do not treat shocks per se. The physical picture is simply that if the apex is driven

supersonic or super-Alfvenic, then shocks are generated. We believe that this treatment is a reasonable one unless the ambient fields are comparable to or exceed the loop fields (~20G for the supersonic examples). The results are to be interpreted as order-of-magnitude estimates.

Figure 3(a) shows the velocity of the apex for a loop with the initial equilibrium height $Z_0 = 10^5$km, $a_0 = 2 \times 10^4$km and $I_t = 4.5 \times 10^{10}$ A, corresponding to $B_p = 4.5$G and $B_t = 8.1$G. This loop is half a torus ($Z_o = s_o$) with the footpoint separation of $2s_o = 2\times10^5$km. This is a case with relatively weak magnetic fields. The ambient pressure is taken to be $p_a = 2$ dyn cm^{-2} at $T = 2 \times 10^6$K so that the number density is $n \simeq 4 \times 10^9$ cm^{-3}. For this loop, we have $\varepsilon_{cr} \simeq 0.28$ (eq. [23]). The values of ε significantly smaller than ε_{cr} should give rise to instability. Curves 1 and 2 correspond to $\varepsilon(t=0) = 0.01$ and $\varepsilon(t=0) = 0.05$, respectively. The velocity is normalized to the sound speed $C_s \simeq 2.4 \times 10^2$ km sec^{-1}. These curves describe two loops of apparently identical appearance above the photosphere with different initial conditions $\varepsilon(0)$ corresponding to different submerged structures. For Curve 1, the flux enclosed by the entire current distribution is one hundred times what is above the photosphere and for Curve 2, the total flux is 20 times what is above. Because of the low current and weak magnetic field, these loops do not expand rapidly. Although not shown here, these loops continue to expand slowly even after one hour with the major radius reaching 1.5 to 2 times the initial values. The expansion is nearly exponential for the first 20 minutes. In Figure 3(b), the height of the loop apex is show. In general, with other parameters being equal, loops with smaller values of $\varepsilon < \varepsilon_{cr}$ expand more rapidly expand more rapidly to larger values of Z, and in cases where loops can attain "second" equilibrium (see Fig. 4 for an example), they do so later and at larger values of Z. Also, as a loop expands, the expansion tends to slow down because the current and magnetic field decrease and $\varepsilon(t)$ increases, sometimes reaching a second equilibrium. The dashed line describes $a(t)/a_o$, showing that the minor radius expansion is much less than the increase in the apex height.

Figures 4 shows the behavior of a smaller loop with an initial height of $Z_0 = 10^4$km and $R_o = 7.2\times10^3$km with $Z_o/s_o = 1.5$. The footpoint separation is $2s_o = 1.33\times10^4$km with $\theta/\pi = 0.374$. The aspect ratio is taken to be 5 so that $a_0 = 1.4 \times 10^3$km. The current is $I_t = 3.3 \times 10^9$A with $B_p = 4.5$G and $B_t = 8.1$G. For this loop, we find $\varepsilon_{cr} \simeq 0.05$. In this example, we have used $\varepsilon = 0.03$ and the loop is only mildly unstable. The apex

velocity reaches a maximum of ~0.3C_s with a rise time of 7 minutes. The velocity then decreases until the height reaches $Z \simeq 6.5\times10^4$km. Subsequently, the apex executes damped oscillation with a period of ~5 min.

Preceding examples show model loops which are fairly "tall", i.e., with $Z_o \geq s_o$; $Z_o = s_o$ for Figure 3 and $Z_o = 1.5s_o$ for Figure 4. Flatter equilibrium loops ($Z_o < s_o$) are also easy to find. It seems intuitively reasonable (perhaps necessary) that flatter loops should be able to slowly evolve to taller configurations if small changes in parameters are made. This is in fact the case. In Figure 5, we use a loop with $Z_o = 10^4$km, $s_o = 1.25\times10^4$km, $R_o = 1.28\times10^4$km, $R_o/a_o = 5$ and $\varepsilon(t=0) = 0.05$. The current is $I_t = 6\times10^9$A with $B_p = 4.5$G and $B_t = 8.1$G in equilibrium. At t=0, we increase the current I_t from the above equilibrium value by 1%. This, of course, corresponds to increasing the magnetic field twist slightly. (Note that the eqs. (3) and (32) are not limited to equilibrium.) The result shows that the apex rises and executes damped oscillation about 1.16×10^4km. The expansion velocity is small, never exceeding ~0.1C_s. Analogously, if the current is decreased slightly, the height can decrease slowly followed by small amplitude damped oscillation. This behavior suggests that a current loop can evolve to a taller (lower) loop in a quasi-equilibrium manner if the current increases (decreased) slowly.

In general, with all other quantities being equal, smaller unstable loops, have shorter e-folding times (eq. [21]) because of the reduced inertia. Unstable loops with larger currents I_t also have shorter e-folding times because of the increased Lorentz force. In Figure 6, we show an example with larger currents. The loop is not in equilibrium initially. This example may be relevant to a loop which suffers loss of equilibrium. The parameters used are $Z_0 = 10^5$km, $Z_o = s_o$, $a_0 = 10^4$km and $I_t = 10^{11}$A so that $B_p = 20$G and $B_t = 21$G. Curve 1 corresponds to $\varepsilon(0) = 0.01$ and the loop attains Mach 3 in less than one minute. At $t \simeq 18$ min, the apex velocity is approximately $V/C_s \simeq 5$ or $V \simeq 1200$ km s^{-1} and the apex has risen to $Z = 20 \times 10^5$ km. Subsequently, the expansion velocity slowly decreases over tens of minutes as the loop expands. Curve 2 corresponds to $\varepsilon(0) = 0.05$ and the configuration is slower than that described by Curve 1. The apex attains Mach 3, the maximum velocity, in about 5 minutes, also with a sharp rise near $t = 0$. The velocity then slowly decreases to Mach 2 in about 30 minutes as the loop expands. For smaller currents, the velocities are smaller. From Figures 3 - 6, it is clear that curvature force can produce a wide range of behavior.

IV. PHYSICAL IMPLICATIONS AND DISCUSSION

We have described the dynamics of the apex of a model current loop embedded in a background plasma. The structure is such that the semi-toroidal section of the loop is in the upper tenuous plasma while the remainder of the current distribution is embedded in a much denser plasma. The dynamical properties obtained are most applicable to the apex of the semi-toroidal loop. We reiterate that the objective is not to model specific phenomena but to understand the basic effects of curvature forces. For this purpose, we have constructed the model in such a way that the model loop behavior is primarily determined by the curvature forces. In the preceding sections, we have given theoretical and numerical results. Although the results cannot be applied directly to observed solar phenomena because of simplifying assumptions, it is useful to determine the range of expected behavior using parameters compatible with the solar environment.

Observationally, it is not always easy to determine the magnetic structure or its motion. However, signatures of motion may be manifested as heating of coronal gas and moving gaseous material. Here, we will examine some possible observational implications. For this purpose, it is useful to consider the rate at which the magnetic energy is converted to thermal energy via drag. We have calculated the quantity

$$\frac{dE}{dt} = F_d\left(\frac{dZ}{dt}\right)$$

for the model loops described in the preceding section. Here, F_d is the drag force given by equation (30) and dE/dt is the rate at which the ambient gas is heated by drag due to the apex motion. In calculating this quantity, we have assumed that only one third of the semi-torus around the apex is effective in drag heating. As the above expression indicates, the heating rate is proportional to V^3. We have also computed the time-integrated total energy which the magnetic field loses in the form of loop plasma kinetic energy and drag heating. This quantity is essentially equal to the time-integral of dE/dt plus the loop kinetic energy. As pointed out before, the minor radial expansion is found to be much slower than the apex motion so that it is neglected in comparison with the major radial expansion.

Figure 7 shows the energy release rates due to drag for the loop described in Figure 3. For $\varepsilon = 0.01$ (Curve 1), the rate reaches 10^{25} erg s^{-1} at t = 20 min and increases to 10^{26} erg s^{-1} at t = 30 min. During this

time, the major radius increases from $1.15Z_0$ to $1.6R_0$. Before t ~ 20 min, the loop exhibits only slow motion and insignificant energy output. For ε = 0.05 (Curve 2), the loop motion is less pronounced with the energy release rate in the range of 10^{25} erg s^{-1} during t = 20 min to t = 30 min. Figure 7(b) shows the time-integrated energy converted from the magnetic field to thermal and kinetic energy. For ε = 0.01 (Curve 1), the total amount of magnetic energy released in 30 minutes is ~ 1.5×10^{29} erg while, for ε = 0.05 (Curve 2), it is 10^{29} erg. For both cases, roughly one half of the energy is in the form of thermal energy. In Figure 8, we give the energy output profile for the loop described in Figure 6. For this loop, the magnetic field components are ~ .706 and the apex can be driven supersonic with correspondingly greater magnetic energy release. However, as discussed before, this loop is not initially in equilibrium in the context of the present model. For Curve 1 (ε = 0.01), the maximum energy release rate is roughly 4×10^{28} erg s^{-1} with a time integrated total of 6 $\times 10^{31}$ erg in 30 minutes. Curve 2 (ε = 0.1), shows an energy output profile in which the peak heating occurs in a duration of 10 minutes with a long decay phase lasting for tens of minutes. The total energy released is roughly 3×10^{31} erg in 30 minutes. For these curves, there is a possibility of strong shock heating. Note that magnetic energy conversion takes place on the time scale of tens of minutes. The rate of energy release can have a wide range. This type of "dynamical" magnetic energy release mechanism has been suggested earlier (Zhu and Chen, 1980). As mentioned earlier, the importance of mechanical energy output in the flare energy budget has been discussed (Webb et al., 1980). Also, if a large number of loops release energy at slow rates, they may contribute to non violent thermal energy input to the corona.

It is of interest to estimate the temperature of the ambient gas which is heated by the supersonic motion of the apex. For strong shocks, the temperature $T_\star$ behind the shock front can be estimated by

$$\frac{T_\star}{T_a} = \frac{[2\gamma M^2 - (\gamma - 1)][(\gamma - 1)M^2 + 2]}{(\gamma+1)^2 M^2} ,$$

(Landau and Lifshitz, 1959) where M is the Mach number of the shock and T_a is the ambient temperature. Taking M ~ 3 (Fig. 6(a)) and $\gamma = 5/3$, we find $T_\star = 3.7\ T_a$. Using $T_a = 2 \times 10^6$ K, we find $T_\star = 7.4 \times 10^6$ K. For larger values of M, the temperature is higher. Thus, in this particular example

(Curve 2), the coronal gas in the vicinity of the apex could be heated to approximately 10^7 K and the heated gas might be seen to travel away from the sun with a peak value of ~ 800 km sec^{-1}. This phase can last for tens of minutes with the velocity and heating diminishing with time. For Curve 1, the velocity is considerably higher (a peak value of ~ 1200 km s^{-1}). These calculated apex velocities are similar to those associated with certain dynamical effects. For example, the sources of moving type IV bursts are quoted to have velocities in the range of roughly 200 km s^{-1} to 1500 km s^{-1} with typical velocities around 400 km s^{-1} (e.g., Svestka, 1980). For coronal mass ejection events, Gosling et al. (1976), for example, reported speeds ranging from less than 100 km s^{-1} to more than 1200 km s^{-1} with the average being roughly 500 km s^{-1}. They also reported association of type II radio bursts with events moving faster than about 400 km s^{-1}. Note that we do not attempt to "explain" these phenomena here.

Mouschovias and Poland (1978) and Anzer (1978) have described loop-type (as opposed to "bubble") transient models. In anzer's work, poloidal current density J_p and plasma pressure are neglected, effectively treating the loop as a metallic wire. The loops are not not in equilibrium initially. In addition, the ambient plasma is neglected. Nevertheless, the underlying physics is similar to that of our model in that both models use Lorentz curvature forces to drive current loops. Here, although the present model is not specifically for coronal transients, we make a qualitative comparison with the work of Anzer. In Anzer's work, it was found that magnetic fields of 1G can drive coronal transients. In our model, we estimate the necessary magnetic fields to be greater. This can be understood in the following way. In Anzer's model, the poloidal current density J_p and pressure gradient are neglected. In the toroidal geometry, the force $J_p B_t$ acts to counter the expansion of the apex. Furthermore, the ambient material which also acts to oppose the expansion is neglected. The only retarding force is gravity. In our present model, we include the poloidal current and plasma pressure. For the nonequilibrium examples (Figs. 6 and 8), the magnetic field components are 10^{-2}-10^{0}G in the lower corona so that gravity is unimportant (see below). Thus, Anzer's model tends to require smaller magnetic fields than our model to drive current loops to a given velocity. In addition, the current loops used by Anzer are much larger, initially ~ $0.5R_\odot$. In our model, the magnetic field is also weaker at comparable altitutes. Taking, for example, Curve 1 of Figure 6, we find that at t ~ 30 min, $Z_o \simeq 3R_\odot$, the magnetic field

components are roughly 10G. For Curve 2 at t = 30 min, $Z_0 \approx 2R_\odot$, the magnetic field components are roughly 5G. We attribute the numerical differences primarily to the neglect of poloidal current and plasma pressure. In addition, the inclusion of ambient coronal gas allows conversion of magnetic energy to thermal energy in our model.

Citing the result of Anzer (1978), Carlqvist and Alfven (1980) suggested that expanding current loops may contribute to the acceleration of solar wind particles. By virtue of including both toroidal and poloidal current components, plasma pressure and ambient gas, our model can be extended to give a potentially better description of loop structure and dynamics beyond the immediate vicinity of the sun. (Also include eq. [33] if gravity is important.) We note that Klein and Burlaga (1982) reported observational evidence of magnetic clouds at 1AU consistent with the geometry of magnetic loops. It has been suggested (Cocconi et al., 1958; Gold 1959, 1962) that the magnetic field lines of magnetic clouds may be anchored in the sun. However, the detailed magnetic structure and dynamics of magnetic clouds in the interplanetary space have not been fully understood. It is possible that expanding current or magnetic loops can naturally give rise to these structures. It is significant to note that Klein and Burlaga (1982) suggested that certain different types of clouds may be different manifestations of a single phenomenon such as coronal transients.

The motion to flux tubes at the base of the convection zone has been considered (Chou and Fisher, 1981; Fisher and Chou, 1982). If such flux tubes are anchored below the convection zone, then equilibrium and dynamical considerations described here and in Xue and Chen (1980; 1983) may be applicable. In particular, the inductive effects described by ε may be relevant.

In the examples treated in this paper, the role of gravity has not been considered. For some phenomena, gravity may be important. For the apex of a loop, gravity acts along the major radius so that it is straightforward to include the gravitational force F_G there

$$F_G = \pi a^2 m_i g (n_a - n). \qquad (34)$$

Here, F_G is the gravitational force per unit length acting on the apex and g is the gravitational acceleration. For the sake of generality, we have included both the ambient density n_a and the average internal density n.

If $\bar{n} > n_a$ (e.g., coronal mass ejections), F_G is downward. If $\bar{n} < n_a$, then the structure is buoyant and F_G is upward. For magnetic fields of 10 - 20G, the curvature forces dominate the gravitational force. For example, for the supersonic loop depicted in Figure 6 with a density of $10^9 cm^{-3}$, the curvature forces are of the order of $10^{10} dyn\ cm^{-1}$ while F_G is of the order of $10^8 dyn\ cm^{-1}$. The basic tenets of curvature effects remain qualitatively valid with the addition of gravity.

In summary, we have theoretically studied the behavior of a simple semi-toroidal current loop under the action of curvature forces. It has been shown that such loops are capable of exhibiting a wide range of dynamical behavior. Starting with MHD equilibria with the curvature forces explicitly balanced and with the footpoints of the loop remaining stationary, loops can expand with a wide range of subsonic velocities, giving rise to a correspondingly wide range of magnetic energy output. Some loops can attain second equilibria. Loops may also evolve, in a quasi equilibrium manner, from "flat" to "tall" loops if the current is increased slowly. The typical time scales for motion and energy release are tens of minutes. Given loops initially in equilibrium with no ambient magnetic fields, the subsequent motion seems to be subsonic with relatively slow heating of the coronal gas. If we start with nonequilibrium loops with large currents, possibly as a result of loss of equilibrium, they can attain highly supersonic (or super-Alfvenic in magnetized ambient plasmas) expansion velocities with rapid heating due to shock heating. Thus, it appears that expansion of magnetic loops can contribute energy to the coronal gas, along with other possible mechanisms, with a wide range of energy release rates.

A novel but somewhat unconventional feature of the model is the inclusion of submerged current distributions in the dynamics of the loop. As pointed out previously, the present model depends on the existence but not any details of the submerged current distributions. The submerged current is parametrized by the quantity ε, the ratio of fluxes, defined by equation (14). Although not measurable in reality, this is a physically meaningful quantity. The condition for instability is found to be given by $\varepsilon < \varepsilon_{cr}$. It is of interest to speculate on how such an equilibrium loop can be manufactured by the sun since a loop which is observed to exist for an extended period of time (perhaps a few days) is presumably in stable equilibrium. For example, if a flux loop emerges through the photosphere, it expands until it reaches an equilibrium for which $\varepsilon > \varepsilon_{cr}$. Recall that

ε_{cr} depends only on physical parameters above the photosphere while $\varepsilon = \Phi_p/\Phi_T$. It is possible within the context of this model that a stable loop can become unstable if Φ_T increases (smaller ε). This may occur due to topological changes in the subphotospheric magnetic flux structure to which the loop is connected. There need not be significant changes in the loop parameters or coronal conditions prior to the onset of expansion.

In our model, the current loop above the photosphere is connected to the submerged structure via flux tubes going through the photosphere. The flux tubes serve as a conduit for electromagnetic and other processes. We have not addressed issues concerning the details of possible flux structures below the phtosphere and possible dynamics of and transport mechanisms in such current or flux structures in subphotospheric regions. It appears that these properties can influence the dynamics of the current loop above. Thus, in a more complete model, the parameter ε will contain much more physical effects. In our calculation, we kept only one aspect, viz., the relative flux and the inductive effects, to illustrate certain basic physical properties. An adequate discussion of these issues requires more understanding of subphotospheric fields and plasma properties, both inside and outside of possible flux structures. As a first step, we have included the submerged current structure only as a parameter. Nevertheless, the basic conclusion that the behavior of current loops can depend on submerged current structures is not based on detailed assumptions and seems worthy of more detailed consideration.

As a starting point for studying the effects of curvature forces, we have used a simple model system in the limit of zero background magnetic field. Although these equilibria ($\beta_p < 0$) may be relevant to certain structures such as "cool loops" with a pressure deficit inside (e.g., Foukal 1976; Chiuderi et al., 1977; Hood and Priest 1979), many of the observed loops are likely to correspond to the $\beta_p > 0$ case. In an upcoming paper, we will report on loop equilibria with nonzero background magnetic fields such that $\beta_p > 0$. The present analysis can be applied to this case in a similar way. One difference is that greater amounts of current can be supported in equilibrium and a wider range of expansion motion can be exhibited by equilibrium loops. The basic effects of curvature forces are not limited to the particular class of equilibria used in this paper.

Throughout the paper, the emphasis and the objective have been to isolate the essential physics of curvature forces and to describe the range of possible behavior that may be exhibited by current loops. The results are to be taken in an order-of-magnitude sense. The effects of various approximations and different types of equilibria should be studied for a more complete understanding. In this paper, we do not claim to explain any particular observed phenomena. The precise role and the relative importance or unimportance of curvature forces in any observed phenomenon must be evaluated in future research. Our reference to observations is limited to pointing out the possible relevance to the solar environment. Nevertheless, it appears that current loops under the action of curvature forces can exhibit a range of motion (velocities, energy dissipation, etc.) in the right "ball park" in the context of dynamical solar phenomena.

Acknowledgments

This work was supported by the Office of Naval Research.

References

Anzer, U. 1978, Solar Phys., 57, 111.

Anzer, U. and Poland, A.I. 1979, Solar Phys., 61, 95.

Bateman, G. 1978, MHD Instabilities, The MIT Press, Cambridge, MA.

Carlqvist, Carlqvist, P. and H. Alfven 1980, Astrophys. Space Sci., 71, 203.

Chen, J. 1987, NRL Memorandum Report 6086 (submitted for publication).

Chiuderi, C., Giachetti, R., and Van Hoven, G. 1977, Solar Phys., 54, 107.

Chou, D.-Y. and Fisher, G. H. 1987, Solar Physics Division Meeting, American Astronomical Society, Honolulu, Hawaii.

Cocconi, G., Gold, T. Greisen, K., Hayakawa, S. and P. Morrison 1958, Nuovo Cimento, 8, 161.

Fisher, G. H. and Chou, D.-Y. 1987, Solar Physics Division Meeting, American Astronomical Society, Honolulu, Hawaii.

Foukal, P. V. 1976, Astrophys. J., 210, 575.

Gold, T. 1959, J. Geophys. Res., 64, 1665.

Gold, T. 1962, Space Sci. Res., 1, 100.

Gosling, J. T., Hildner, E., MacQueen, R. M., Munro, R. H., Poland, A. I., and Ross, C. L. 1976, Solar Phys., 48, 389.

Hildner, E. 1977, L. D. de Feiter Memorial STIP Symposium, Tel Aviv.

Hood, A.W. and Priest, E. R. 1979, Astron. Astrophys., 77, 233.

Hoerner, S. F. 1951, Aerodynamic Drag, Otterbein Press, Dayton, Ohio, P. 223.

Klein, L. W. and Burlaga, L. F. 1982, J. Geophys. Res., 87, 613.

Landau, L. D. and Lifshitz, E. M. 1959, Fluid Mechanics, Pergamon Press Inc., New York, P. 331.

Mouschovias, T. Ch., and Poland, A. I. 1978, Ap. J., 220, 675.

Shafranov, V. D. 1966, in Reviews of Plasma physics, Vol. 2, Consultants Bureau, New York.

Svestka, Z. 1980, in P.A. Sturrock (ed.), Solar Flares, Colorado Assoc. Univ. Press, Boulder, Colorado, P. 95.

Tritton, D. J. 1977, Physical Fluid Dynamics, Van Nostrand Reinhold Co., New York, P. 29.

Van Tend, W. 1979, Solar Phys., 61, 89.

Webb, D. F., Cheng, C.-C., Dulk, G. A., Edberg, S. J., Martin, S. F., McKenna-Lawlor, S., and McLean, D. J. 1980, in P. A. Sturrock (ed.), Solar Flares. Colorado Assoc. Univ. Press, Boulder, Colorado.

Xue, M. L. and Chen, J. 1980, PFC/JA-80-27, Massachusetts Institute of Technology, Cambridge, Mass.

Xue, M. L. and Chen, J. 1983, Solar Phys., 84, 119.

Yeh, T. and Dryer, M. 1981, Ap. J., 245, 704.

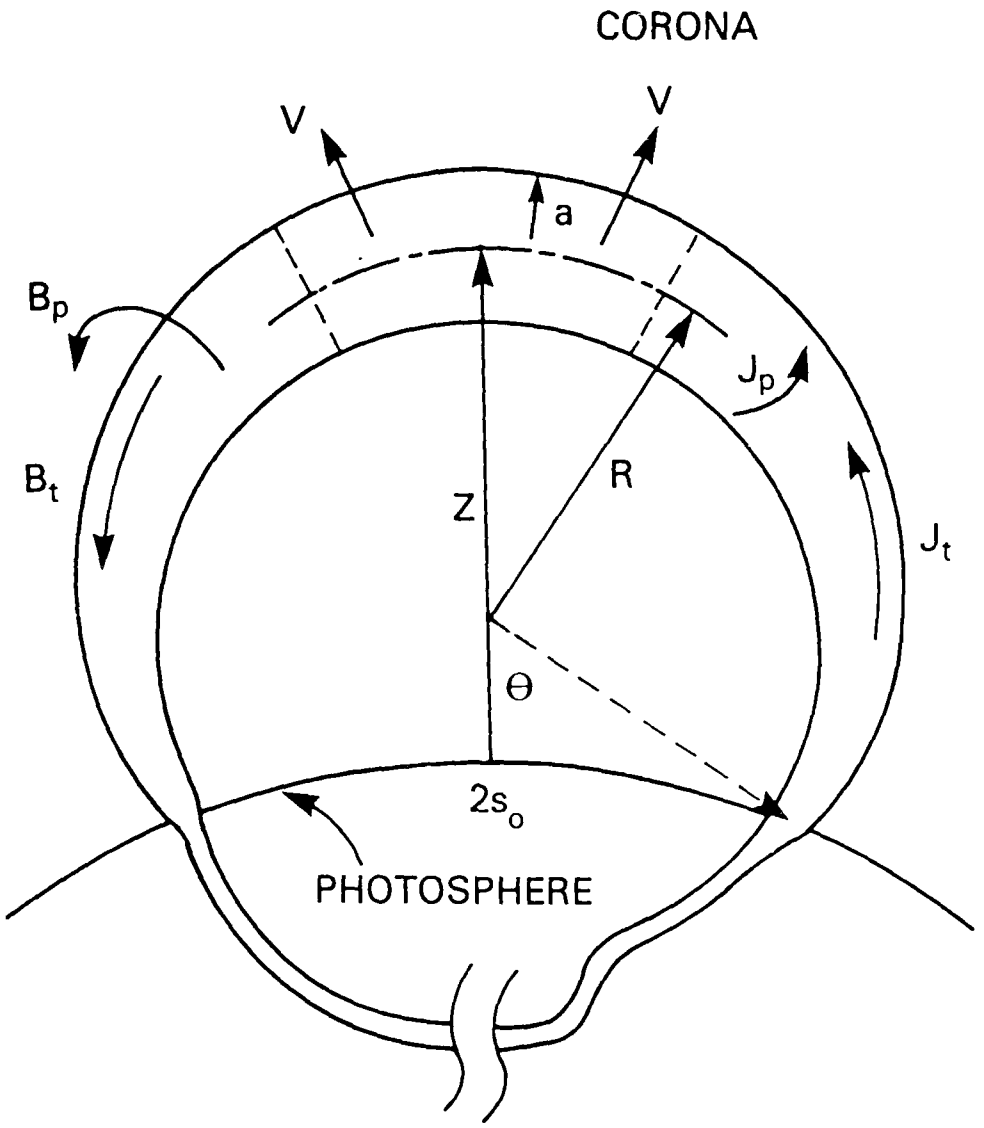

Fig. 1 Schematic drawing of a model current loop embedded in the corona. Components of the current density $\underline{J}$ and magnetic field are shown. The subscripts "t" and "p" refer to the toroidal and poloidal directions, respectively. The radius of curvature is R and the apex height from the photosphere is Z. The footpoint separation is $2s_o$. The segment between the dashed lines is the "apex region", taken to be 1/3 of the loop for numerical calculations (Secs. III and IV). If the apex region were devided into thin slices, the center of mass of each slice would lie on the dash-dot line. No particular structure is specified below the photosphere.

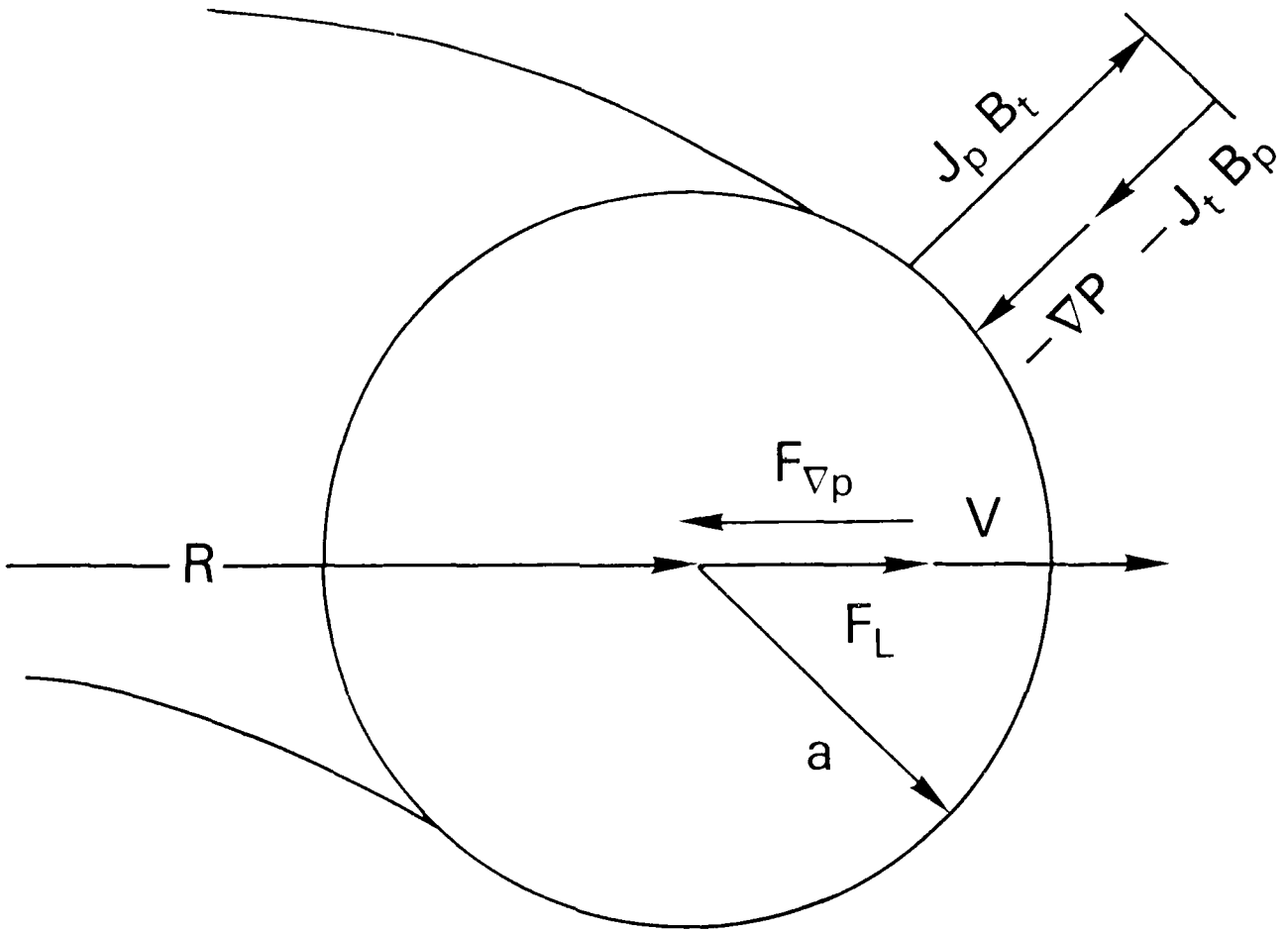

Fig. 2 Forces acting on a toroidal current loop. The components $J_p B_t$, ∇p, and $J_t B_p$ act along the minor radius (a). The "curvature forces" acting along the major radius (R) are $F_{\nabla p}$, the pressure force and F_L, the Lorentz force. The drag force F_d acts in the opposite direction to $\underline{V}$.

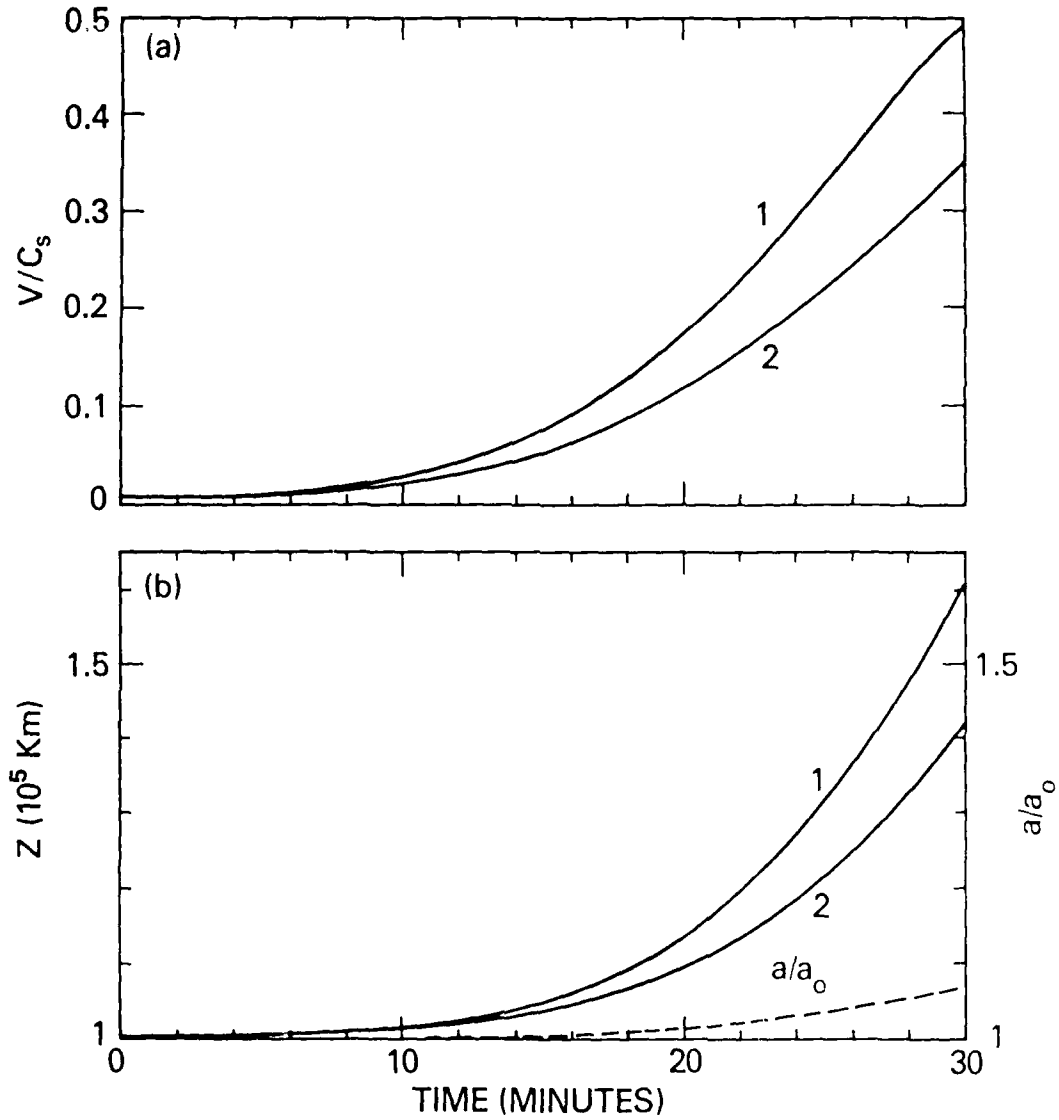

Fig. 3 Behavior of a model loop initially in equilibrium with $Z_o = 10^5$km, $Z_o = s_o$ and $a = 2 \times 10^4$km. $\varepsilon_{cr} = 0.28$ (eq. [23]). $I_t = 4.5 \times 10^{10}$A, $B_p = 4.5$G and $B_t = 8.1$G. For both figures, Curve 1 is $\varepsilon(t=0) = 0.01$ and Curve 2 is $\varepsilon(t=0) = 0.05$. (a) Velocity profile normalized to the sound speed $C_s \tilde{=} 2.4 \times 10^2$ km sec^{-1}. (b) Apex height. The dashed line shows $a(t)/a_o$ corresponding to Curve 1.

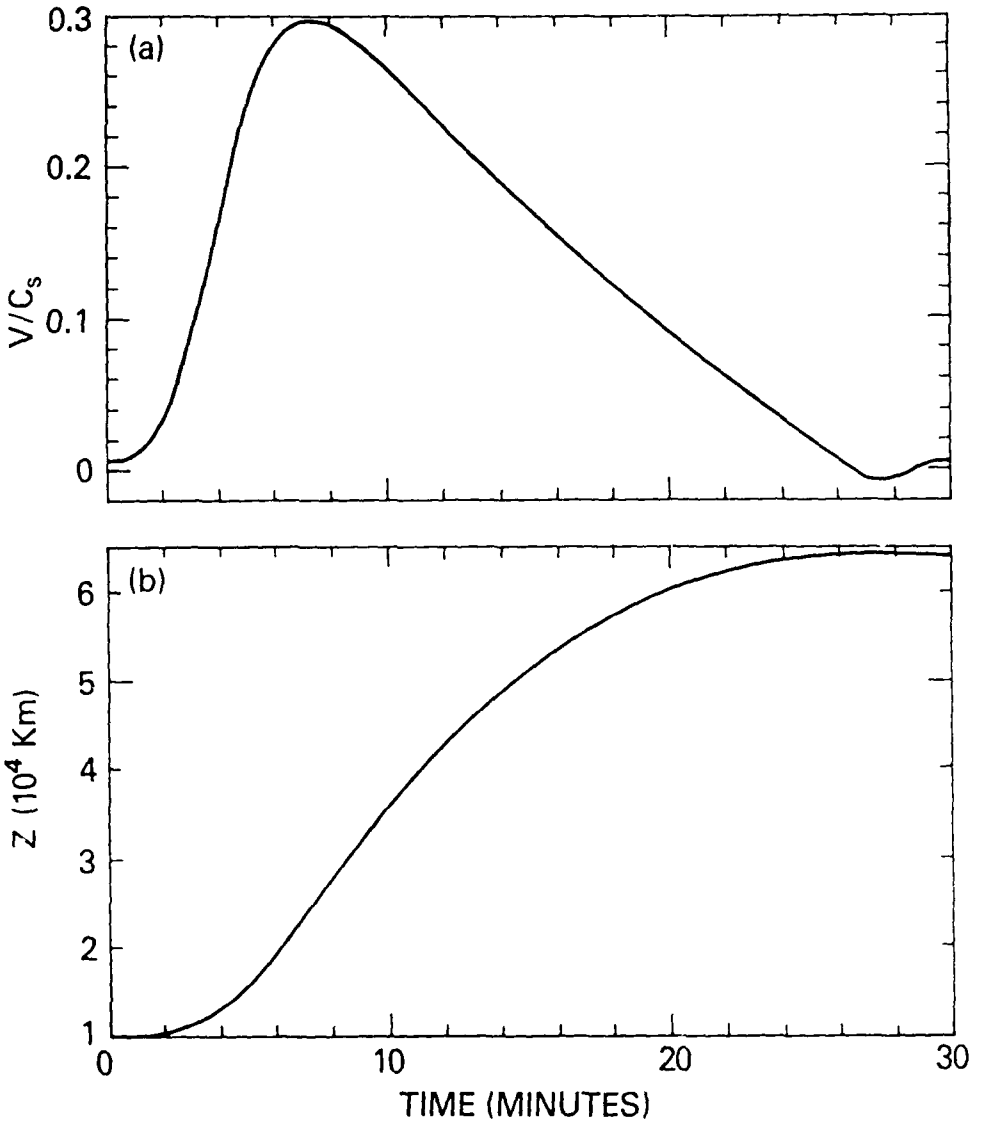

Fig. 4 Behavior of a model loop initially in equilibrium with $A_o = 10^4$km, $s_o = Z_o/1.5$ and $a_o = 1.4 \times 10^3$km. $I_t = 3.3 \times 10^9$A, $B_p = 4.5$G and $B_t = 8.1$G. $\varepsilon_{cr} = 0.05$ and $\varepsilon(t=0) = 0.03$. (a) Velocity profile. (b) Apex height.

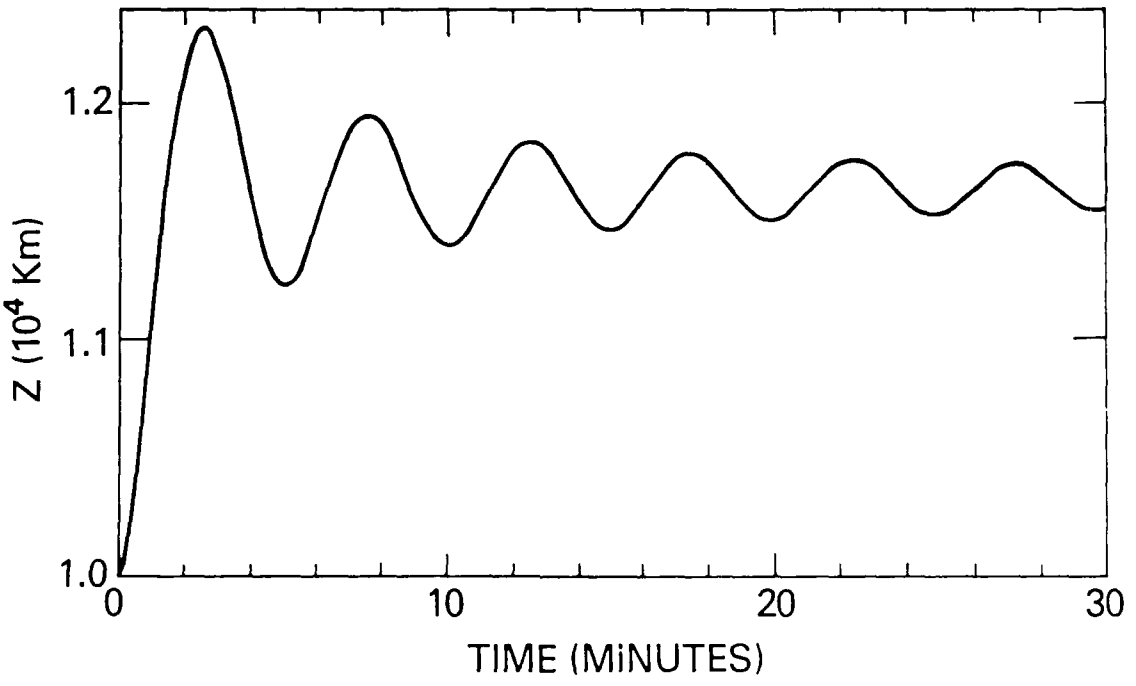

Fig. 5 Height of the apex of a quasi-equilibrium model loop with $Z_o = 10^4$ km, $Z_o = 0.8s_o$ with $s_o = 1.25\times10^4$km and $a_o = 2.6\times10^3$km. $I_t = 6\times10^9$A, $B_p = 4.5$G and $B_t = 8.1$G. The curve corresponds to $\varepsilon(t=0) = 0.05$.

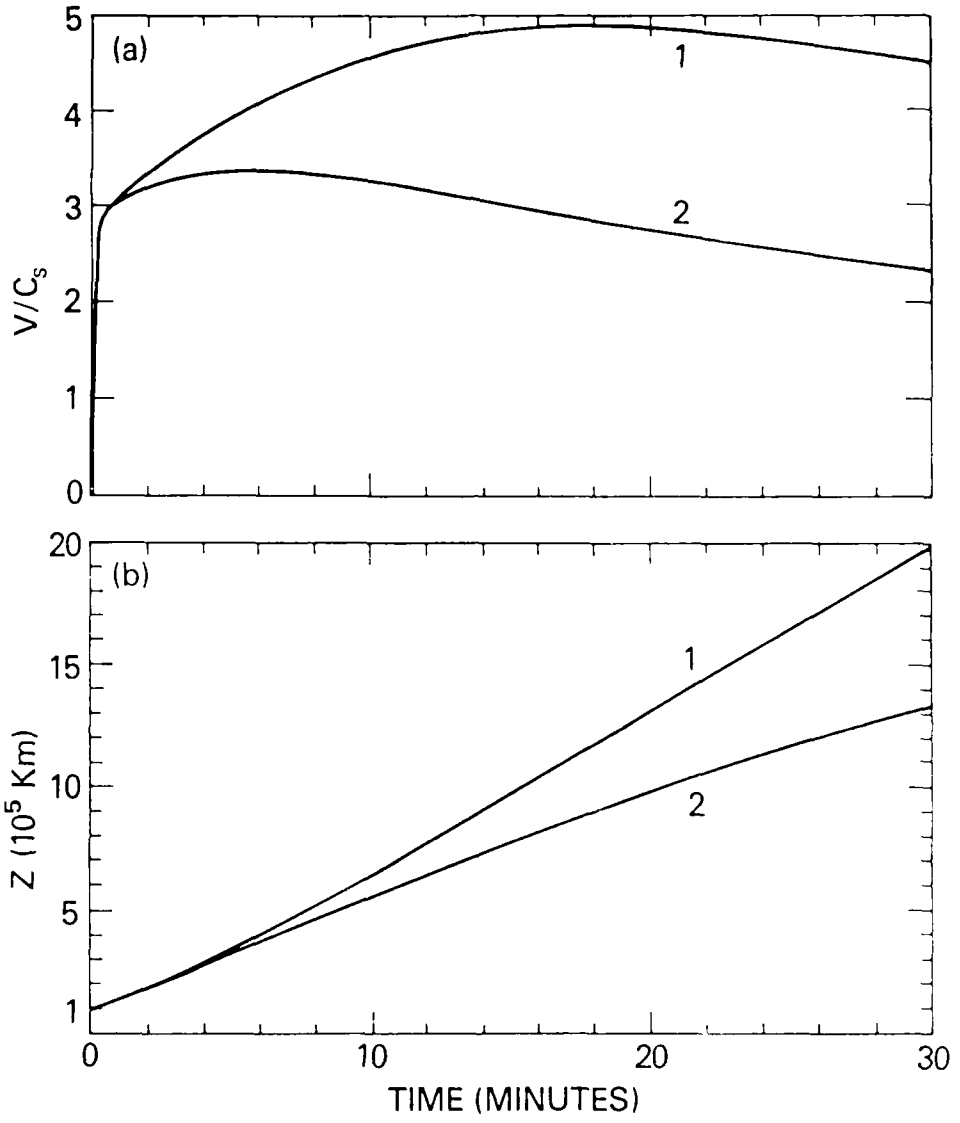

Fig. 6 Behavior of a nonequilibrium model loop with $Z_o = s_o = 10^5$km and $a_o = 10^4$km. Curve 1 is $\varepsilon = 0.01$ and Curve 2 is $\varepsilon = 0.05$. The quantity ε_{cr} does not apply to nonequilibrium loops. $I_t = 10^{11}$A, $B_p = 20$G and $B_t = 21$G. (a) Velocity profile. (b) Apex height.

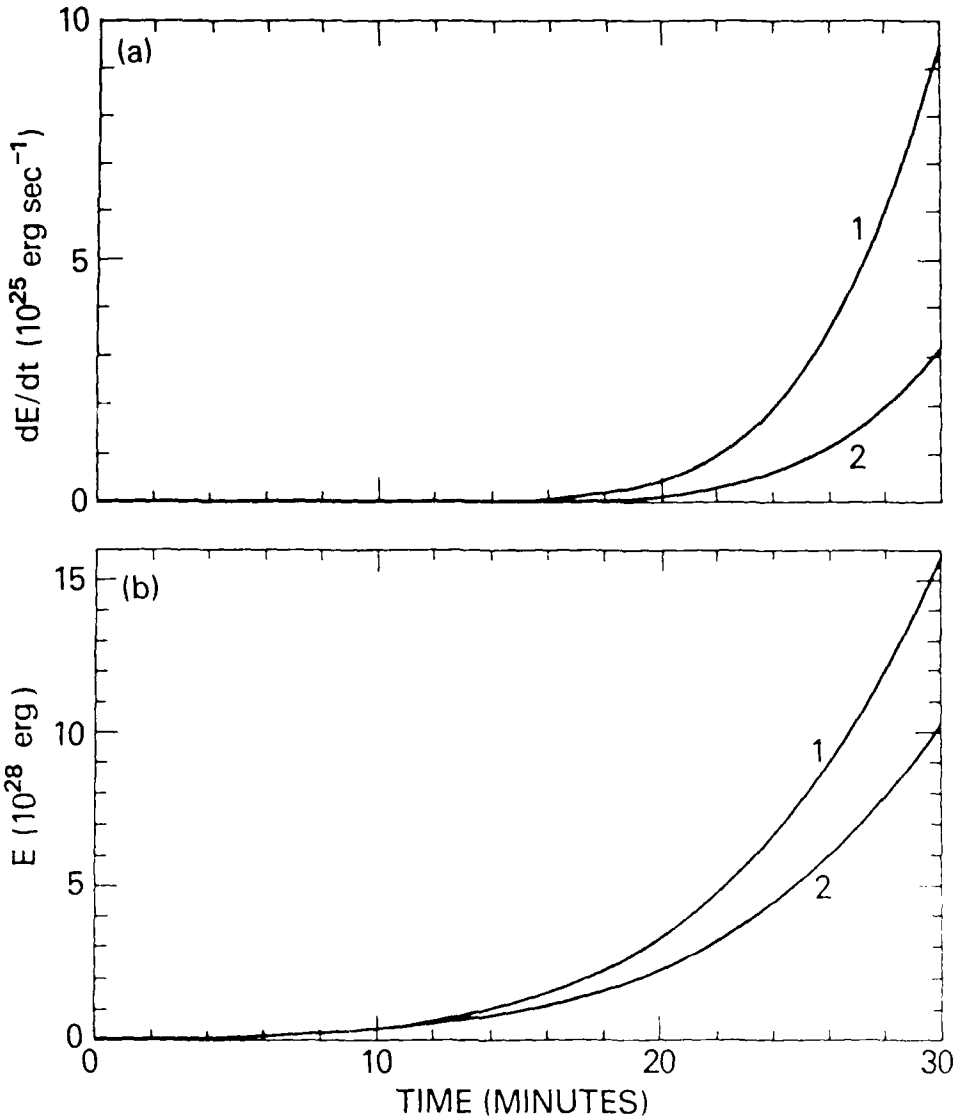

Fig. 7 Magnetic energy released by the model loop of Fig. 3 ($R = 10^5$ km and $a = 2 \times 10^4$ km). Curve 1 is $\varepsilon = 0.01$ and Curve 2 is $\varepsilon = 0.05$. (a) Rate of drag heating near the apex. (b) Time integrated magnetic energy released as drag heating and kinetic energy. Drag heating is roughly one-half of the total energy released.

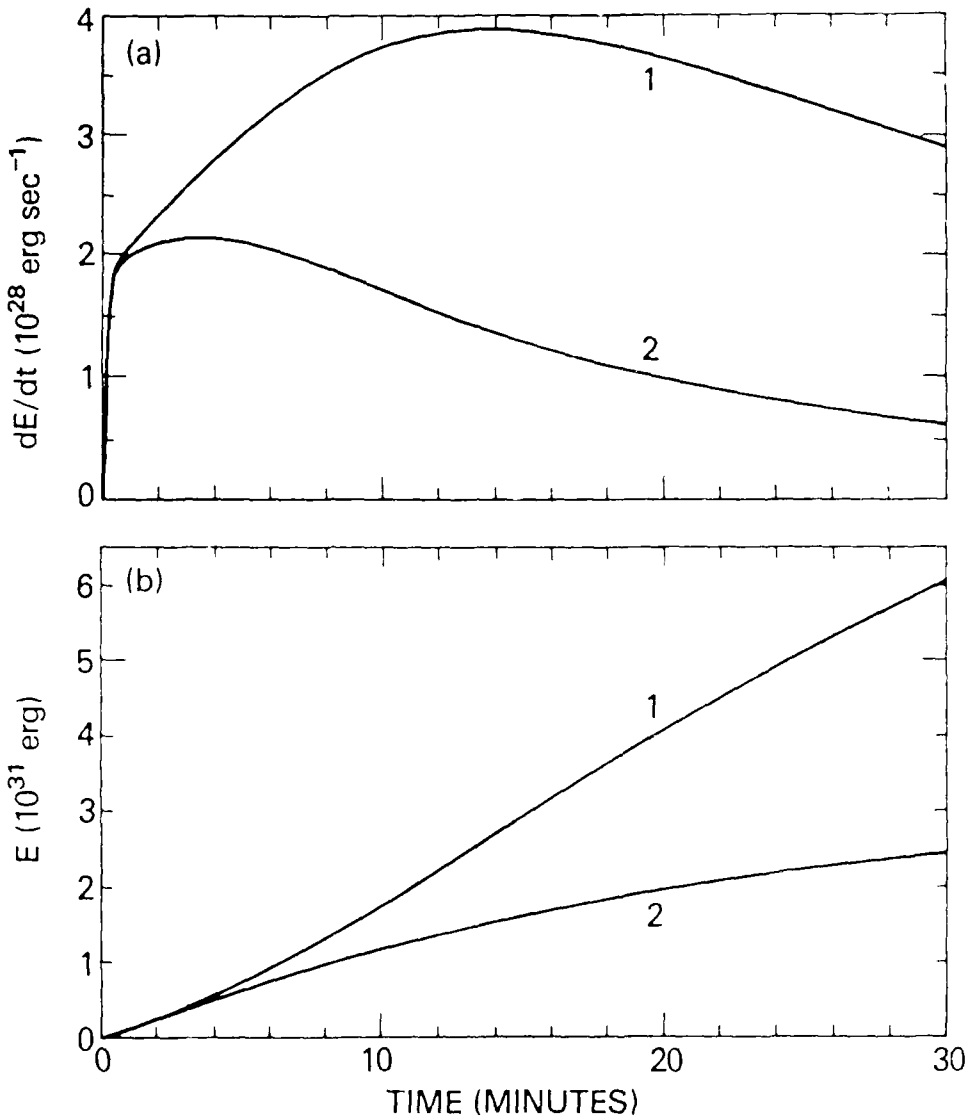

Fig. 8 Magnetic energy released by the nonequilibrium loop of Fig. 6 (R = 10^5 km and a = 2 x 10^4 km). Curve 1 is ε = 0.01 and Curve 2 is ε = 0.01. (a) Rate of drag heating near the apex. (b) Time integrated magnetic energy released as drag heating and kinetic energy.


DATE
FILMED
2-8